Photoelectron imaging of XUV photoionization of CO2 by 13–40 eV synchrotron radiation

Federico J. Furch, Sascha Birkner, Julia H. Jungmann, Freek Kelkensberg, Claus Peter Schulz, Arnaud Rouzée, and Marc J. J. Vrakking

---

Articles you may be interested in

Isotope effects and spectroscopic assignments in the non-dissociative photoionization spectrum of N2
J. Chem. Phys. **140**, 194303 (2014); 10.1063/1.4873717

Rotationally resolved vacuum ultraviolet pulsed field ionization-photoelectron vibrational bands for H D + (X Σ g + 2 , v + = 0 − 20)
J. Chem. Phys. **126**, 164303 (2007); 10.1063/1.2720843

Rotationally resolved pulsed field ionization photoelectron study of CO + (X 2 Σ + ,v + =0–42) in the energy range of 13.98–21.92 eV
J. Chem. Phys. **111**, 8879 (1999); 10.1063/1.480259

A high-resolution vacuum ultraviolet photoionization, photoelectron, and pulsed field ionization study of CS2 near the CS 2 + (X 2Π3/2,1/2) thresholds
J. Chem. Phys. **106**, 864 (1997); 10.1063/1.473967

A study of the SO molecule with photoelectron spectroscopy using synchrotron radiation
J. Chem. Phys. **106**, 821 (1997); 10.1063/1.473227

Photoelectron imaging of XUV photoionization of CO_2 by 13–40 eV synchrotron radiation

Federico J. Furch,[1,2] Sascha Birkner,[1] Julia H. Jungmann,[2] Freek Kelkensberg,[2] Claus Peter Schulz,[1] Arnaud Rouzée,[1] and Marc J. J. Vrakking[1,2]

[1]*Max Born Institute, Max-Born-Str. 2a, 12489 Berlin, Germany*
[2]*FOM-Institute AMOLF, Science Park 104, 1098 XG Amsterdam, The Netherlands*

Valence band photoionization of CO_2 has been studied by photoelectron spectroscopy using a velocity map imaging spectrometer and synchrotron radiation. The measured data allow retrieving electronic and vibrational branching ratios, vibrationally resolved asymmetry parameters, and the total electron yield which includes multiple strong resonances. Additionally, the spectrum of low kinetic energy electrons has been studied in the resonant region, and the evolution with photon energy of one of the forbidden transitions present in the slow photoelectrons spectrum has been carefully analyzed, indicating that in the presence of auto-ionizing resonances the vibrational populations of the ion are significantly redistributed. © *2013 AIP Publishing LLC*. [http://dx.doi.org/10.1063/1.4820947]

I. INTRODUCTION

The application of spectroscopic methods using absorption, emission, and scattering of light is one of the most powerful ways to access information about molecular structure and dynamics. Additionally, photoelectron spectroscopy (PES) has been widely employed to understand, among other things, the dynamics of photoionization in molecules, including the decay of super-excited states by auto-ionization. Carbon dioxide (CO_2) has been one of the most widely studied molecules, due to its importance in biology and in the terrestrial atmosphere, and consequently its impact on the planet's climate. Selected examples may be found in Refs. 1–10.

The advent of new laser technology capable of generating attosecond laser pulses (1 as $= 10^{-18}$ s) in the extreme ultraviolet (XUV) part of the electromagnetic spectrum, has enabled the observation and control of electronic processes with attosecond time resolution.[11] Consequently, spectroscopic knowledge on XUV-induced molecular processes has acquired a new relevance. For example, the population of electronic and vibrational states of both the molecular ion and super-excited states of the neutral molecule following excitation by XUV light is essential for the analysis of pump-probe experiments that are currently being performed, where molecular excitation by an attosecond XUV pulse is followed on ultra-short timescales by a probe pulse that allows observing the molecular dynamics that results from the XUV excitation.[12,13] Additionally, the values of cross sections, electronic and vibrational branching ratios and asymmetry parameters allow the validation of advanced computer codes that support the interpretation of attosecond pump-probe experiments as well as related strong field ionization and high-harmonic imaging experiments.[14,15] In these experiments, both coupling of the electronic and nuclear degrees of freedom and multi-electron correlations cannot be neglected and in most cases are of fundamental importance for the understanding of the experimental results.

A large number of experimental approaches have already been applied to study XUV-induced photoionization. Here, we focus on the potential of Velocity Map Imaging (VMI) spectrometry,[16] which in combination with a source of tunable photon energy, such as a synchrotron, offers the possibility of recovering most of the information offered by other techniques, in a single, simple experiment. The unit collection efficiency and high resolution of VMI at low electron or ion kinetic energy, as well as its inherent capability to obtain angular information, make VMI a very suitable technique to study XUV-induced photoionization.[17,18]

In this paper, we report experiments on XUV photoionization of CO_2 carried out at the BESSY II synchrotron facility at the Helmholtz Zentrum Berlin (HZB). Detection of photoelectrons utilizing a VMI spectrometer with an integrated gas injection system[19] allowed performing extensive, high quality experimental investigations of various molecular samples. More specifically, angle-resolved photoelectron kinetic energy distributions were recorded for CO_2 from the ionization threshold to a photon energy of approx. 40 eV in steps of 20 meV. Additional measurements with 2 meV steps in photon energy were performed in a region where resonant effects produce steep variations in the cross sections and angular distributions, which for CO_2 comprises roughly the region from 14.5 eV to the ionization threshold of the C-band, above 19 eV. We compare our results to the existing literature and provide new information on the evolution of electronic and vibrational branching ratios and asymmetry parameters. In particular in regions with auto-ionizing resonances, we observe strong contributions from Franck-Condon forbidden transitions to the total ionization cross section.

II. EXPERIMENTAL PROCEDURE

A. Set-up

The experiments were performed at the U125-2-10m-NIM undulator beamline of the BESSY II synchrotron at HZB. This beamline delivers electromagnetic radiation in the energy range between 8 and 40 eV that is monochromatized using a 10 m normal incidence monochromator. More details on the beamline can be found in Refs. [20] and [21] The resolution of the monochromator was matched to the photon energy steps of the scans. After the monochromator, the horizontally polarized XUV beam was focused into the VMI spectrometer by a toroidal mirror. Before entering the interaction chamber, a knife edge was used to block scattered light originating from the optics of the beamline. If left unblocked, part of this scattered light impinges on the repeller electrode, leading to a strong background signal. The spot size at the focal point was estimated to be $100 \times 100 \ \mu m^2$ at 25 eV, weakly changing with the photon energy. The relative wavelength-dependent photon flux was measured using a calibrated photodiode, thereby accounting for the combined effect of the undulator, the monochromator, and the focussing optics. These data and the ring current of the synchrotron, which slowly vary over the course of longer measurements, were used to calibrate the electron yields.

The kinetic energy and angular distribution of photoelectrons resulting from photoionization of CO_2 were measured using a VMI spectrometer based on the early design of Eppink and Parker.[16] We used an advanced version with an integrated, continuous gas injection system, which has been described in detail in Ref. [19]. In this VMI, the gas enters the interaction region through a pinhole (12 μm diameter) in the repeller electrode, which is located very close to the interaction region and which has a conical shape to maintain, as much as possible, the optimal electrostatic fields for velocity mapping. This approach strongly enhances the gas density in the interaction region and correspondingly leads to much higher count rates than in traditional VMI designs utilizing a skimmed molecular beam. During the course of the experiment, the pressure in the VMI chamber was limited to 10^{-6} mbar to avoid deterioration of the micro-channel plate detector at high voltage. Considering a pumping speed of 450 l/s, approximately 1.1×10^{16} molecules/s could be introduced into the vacuum chamber. In order to avoid unwanted photoelectron emission from the repeller surface, the interaction with the synchrotron beam took place approximately 0.5 mm above the repeller plate and therefore leading to a reduction in gas density down to 1.2×10^{14} molecules/cm^3 (assuming an effusive expansion characterized by a solid angle of 1 steradian, and a molecular velocity of 300 m/s). Using the fact that for 25 eV photons the CO_2 photoionization cross section is 3×10^{-17} cm^2 (Ref. [22]) and the photon flux of the beamline for a bandwidth of a few meV is in the order of 2×10^{11} photons per second, a maximum of $\sim 5 \times 10^7$ photoelectron impacts/second on the detector is expected. Hence, images with very good statistics can be recorded in a matter of seconds, illustrating the potential of the setup. In practice, we worked at a lower count rate of approximately 5×10^4 counts per second to avoid unwanted saturation of the micro-channel
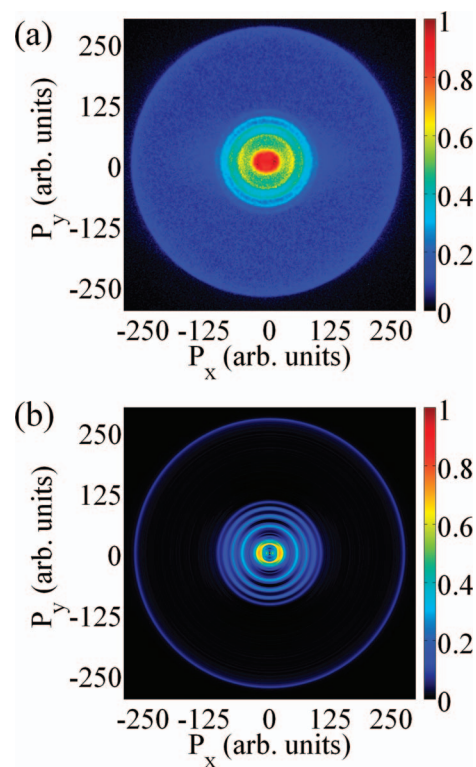

FIG. 1. Experimental image showing the two-dimensional (2D) projection of the electron momentum distribution resulting from 17.91 eV photoionization of CO_2 (a) and a slice through the retrieved 3D momentum distribution (b). P_x is the momentum parallel to the propagation direction of the synchrotron beam, while P_y is parallel to the polarization of the synchrotron beam. The outer ring corresponds to formation of the CO_2^+ molecular ion in the X $^2\Pi_g$ state, while the inner structures reveal the formation of several vibrational levels of the A $^2\Pi_u$ state.

plate detector. An example of the image quality obtained under such conditions is given in Figure 1(a), which shows the two-dimensional (2D) projection of photoelectrons resulting from 17.91 eV photoionization of CO_2.

B. Data evaluation

To retrieve the kinetic energy and angular distribution of the photoelectrons, the measured 2D images were transformed back into a three-dimensional (3D) velocity distribution through an Abel inversion. Since its direct evaluation is numerically challenging, a number of different methods have been developed over the years to do this.[23–25] In the present case, a variant of the method from Ref. [25] was used. In the inversion process, the recorded 2D images were transformed into polar coordinates and for each radius (which is proportional to the modulus of the velocity in the plane of the detector) the experimental angular distribution was fitted to an expansion of Legendre polynomials. Since single photon dipole transitions are studied, it is sufficient to use Legendre polynomials up to second order (P_2) in this fitting procedure. The Legendre polynomial expansion of the 3D momentum distribution was subsequently obtained by applying the inverse of a linear transformation that maps a given cylindrically symmetric 3D distribution onto a 2D plane. Figure 1 shows an example of an experimental image and a slice through the retrieved 3D momentum distribution. Due to the symmetry given by

the polarization axis of the synchrotron light, the right and left halves of the experimental image contain the same information. Most of the results presented here were obtained by averaging over the results from each half.

The experimental kinetic energy resolution was determined by measuring peak widths in photoelectron spectra of Helium, measured at photon energies between 25 and 40 eV. The relative kinetic energy resolution $\Delta E/E$ that can be achieved with a VMI spectrometer depends on the ratio between the smallest spot size that a single velocity can be focussed to and the maximum radius on the micro-channel plate detector where signals can be measured, and can approach $\Delta v/v = 0.5 \cdot \Delta E/E = 0.01$. In practice, the resolution is optimized for a particular energy range. In the configuration utilized throughout the experiment, the resolution changed from $\Delta E/E \approx 0.09$ at 0.4 eV kinetic energy to $\Delta E/E \approx 0.03$ at 4.4 eV and $\Delta E/E \approx 0.04$ at 15.4 eV. Illustrating the kinetic energy resolution of the measurements, the spin-orbit splitting of some vibrational levels ($\approx$10 meV energy separation) could be resolved at low kinetic energies.

The calibration of the photoelectron kinetic energy (KE) was obtained by fitting the change in KE to the change in photon energy during a scan. A small correction offset had to be applied to the value of the photon energy to match the known ionization threshold values of different molecular samples.

III. RESULTS AND DISCUSSION

A. Overview of the data

Figure 2 shows the evolution of the photoelectron spectra determined by angular integration of velocity map images measured for CO_2 from below 13 eV to 41 eV (in steps of 20 meV). Photoelectrons resulting from ionization of the neutral molecule, with electronic configuration $(4\sigma_g)^2(3\sigma_u)^2(1\pi_u)^4(1\pi_g)^4$, to one of the four lowest electronic states of CO_2^+ can be clearly observed, namely: the X $^2\Pi_g$, A $^2\Pi_u$, B $^2\Sigma_u^+$, and C $^2\Sigma_g^+$ states with adiabatic ionization energy (IE) of 13.778 eV, 17.314 eV, 18.077 eV, and

19.394 eV respectively.[26] In the 15–19.4 eV photon energy range, strong resonances are present, which originate from auto-ionizing Rydberg states converging to the A, B, and C bands. The interaction of their vibrational states with the ionic ground and excited states gives rise to an interesting but complex structure which will be discussed further below. Above 19.4 eV photon energy, the photoelectron spectra simplify and the electron yield decreases smoothly towards higher excitation energies without any resonant features. Around 25 eV photon energy and onwards, a weak electron signal appears, with two clear contributions: one around 27–28 eV and another beginning around 32–33 eV. A similar signal has been observed in dipole (e,2e) and synchrotron experiments and was attributed to multi-electron transitions.[27,28]

The spectrum shown in Figure 2 is under-sampled in the region between the ionization threshold and 20 eV, where numerous sharp resonances are present. Therefore, a more detailed scan was performed with 2 meV steps in the region between 14.5 eV and 21.2 eV. These results are shown in Figure 3. The colour scale has been normalized to 1 in each

FIG. 3. Vibrationally resolved photoelectron yield as a function of photon energy for the 4 lowest electronic states of CO_2^+. The experiment reveals numerous auto-ionizing resonances. The insets show cuts through the 3D momentum distributions for selected photon energies. Figure (b) spans a smaller range of photon energies than (a) and therefore the slopes are different. The green vertical lines indicate the onset of the A, B, and C states, respectively.
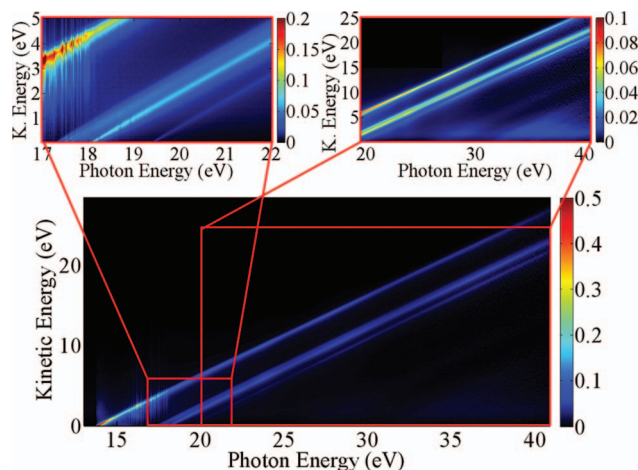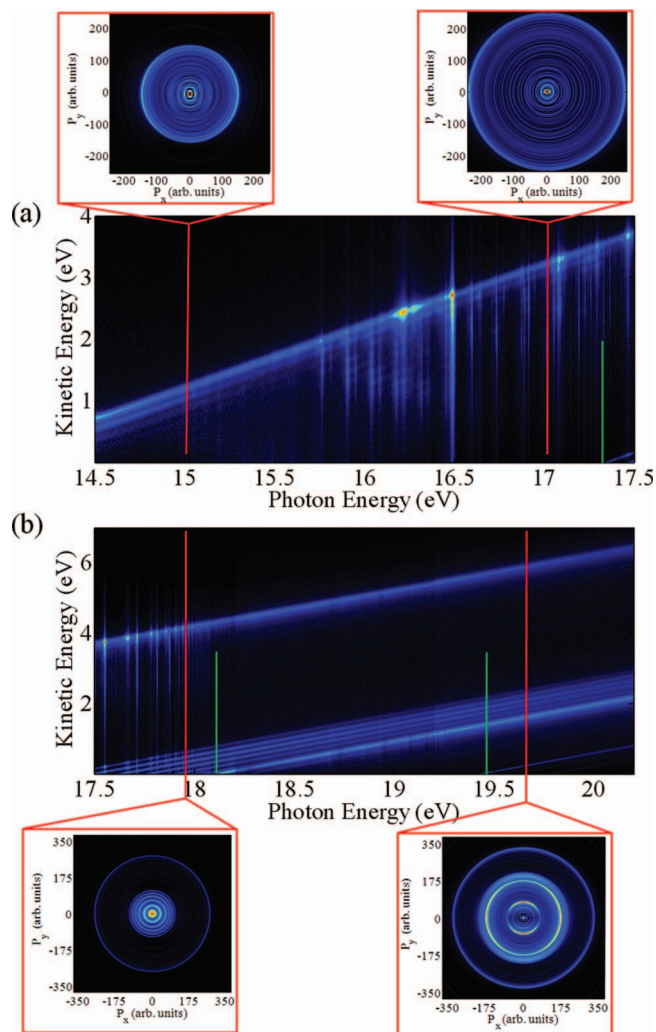

FIG. 2. Photoelectron spectra as a function of photon energy. The electron yield is normalized to the overall maximum value. The two insets show an enlarged view of the photoelectron spectra for the four valence bands of CO_2^+ (left) and the presence of additional contributions originating from multi-electron processes (right).

panel in order to better appreciate the features present in each one of them. Additionally, each subfigure has an inset showing a cut through the retrieved 3D momentum distribution for selected photon energies, illustrating the wealth of information retrieved.

In Figure 3(a), the vibrational structure of the CO_2^+ X $^2\Pi_g$ ground state is clearly visible. The dominant diagonal line with the highest kinetic energy corresponds to formation of the (000) vibrational ground state, which has the largest Franck-Condon overlap with the neutral ground state. The onset of the A $^2\Pi_u$ band is indicated by a vertical green line and its vibrational progression can be followed in Figure 3(b). The onset of the B $^2\Sigma_u^+$ and C $^2\Sigma_g^+$ bands are marked in Figure 3(b) by green vertical lines. Most of the vibrational levels seen in our measurement have been observed and assigned in earlier high resolution photoelectron spectroscopy (PES) measurements with He-I lamps[4, 26, 29, 30] or in threshold photoelectron spectroscopy (TPES) and PES measurements at synchrotron sources.[5–7] In addition to the spectroscopic information on the vibrational structure of CO_2^+, the electron distributions measured with the VMI contain energy-resolved angular distributions and branching ratios between the different electronic and vibrational levels. In Sec. III B, this information will be presented and compared to data available in the literature.

B. Cross section, branching ratios, asymmetry parameters, and slow electrons

1. Total electron yields

Figure 4 shows the total ionization yield that was obtained by integration of the measured kinetic energy distributions for photon energies between 14.8 and 19.1 eV. The total ionization yield displays a complex structure of peaks and shoulders which originate from auto-ionizing resonances. Most of these resonances have been assigned in earlier studies. Thus, we will only give a brief overview of the different series which are observed, following the assignments given by Shaw *et al.*[8]

In the photon energy range between 15.7 eV and 18.0 eV the total ionization yield is dominated by the Tanaka-Ogawa series and the Henning series, denoted in Figures 4(a)–4(c) by red and blue lines, respectively. The Tanaka-Ogawa series is a Rydberg series that arises from the excitation of an electron from the $1\pi_u$ molecular orbital and hence converges to the A $^2\Pi_u$ state. Each member of the Rydberg series exhibits a long vibrational progression $v_1' = 0$ up to 7. Each series consists of two components that converge onto the two spin-orbit split levels of the A state, which are separated by about 10 meV. In our experiments, the splitting of these levels can only be resolved at low kinetic energy electrons (<25 meV). The exact assignment of the Tanaka-Ogawa series is still under debate, but theoretical considerations point to a $nd\delta_g$ configuration.[10] Because of these uncertainties the series has been labelled with a running number *m* instead of the principal quantum number *n* in Ref. 8, which we have carried over in Figure 4. Between 15.8 eV and 16.4 eV, a weak progression labelled "Lindholm" (green lines in Figure 4(a)) ap-
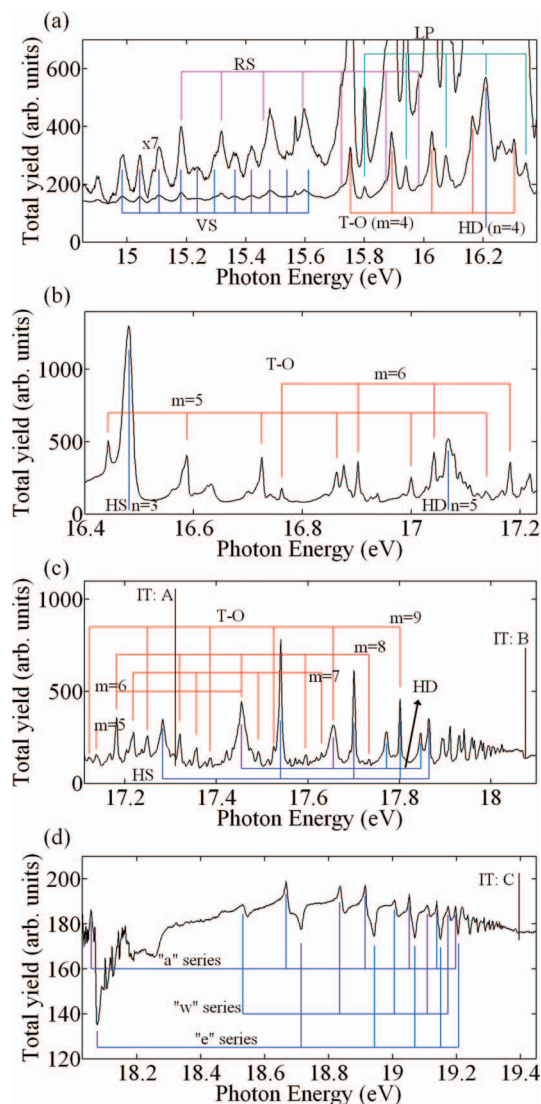

FIG. 4. Total electron yield in the resonant region and line assignments. RS: Rydberg states; LP: Lindholm progression; VS: valence states; T-O: Tanaka-Okawa series; HD: Henning diffuse series; HS: Henning sharp series; and IT: ionization threshold.

pears which has been assigned tentatively to a Rydberg series converging to the A state with nd_g symmetry.[31] The Henning series consists of both sharp and diffuse peaks which converge to the B $^2\Sigma_u^+$ state and have been assigned as $nd\sigma_g$ $^1\Sigma_u^+$ and $ns\sigma_g$ $^1\Sigma_u^+$, respectively.[8, 10] Figure 4(d) shows three Rydberg series denoted as "a", "w", and "e" which converge to the C $^2\Sigma_g^+$ state. The assignment of these series is uncertain, as discussed in Ref. 8.

2. Branching ratios between electronic bands

When the integration is restricted to the photoelectron kinetic energy range covered by a single electronic band, one can determine the partial ionization yield and calculate branching ratios. Figure 5 shows the branching ratios between the X, A, B, and C bands as a function of the photon energy, from the onset of the A band to 40 eV. Figure 5(a) shows the electronic branching ratios in the resonant region between the
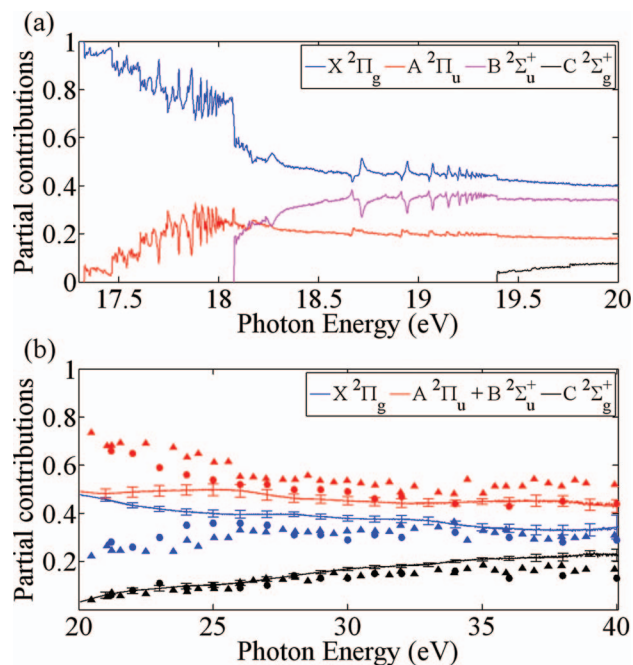
FIG. 5. (a) Electronic branching ratios extracted from the high resolution photon energy scan in the resonant region (Figure 3). (b) Electronic branching ratios extracted from the low resolution photon energy scan (see Figure 2). The solid lines correspond to this work while circles were extracted from Ref. 27 and triangles from Ref. 32.

IE of the A band (at 17.314 eV) and 20 eV using the high resolution photon energy scan shown in Figure 3. In this energy range, the A and the B bands, which are intrinsically mixed, could be distinguished, as long as the overlap of the high-lying vibrational levels of the A band with the B band was ignored. A justification for this lies in the fact that the population of high vibrational levels of the A band lying above the threshold of the B band is much less intense than both the A band population below the B band threshold and the population of the B band itself. Thus, the error imposed by this procedure is negligible compared to the experimental uncertainties. Figure 5(b) shows that the contribution of the B band is much larger than that of the A band. Towards 20 eV the A/B ratio reaches 0.53.

The data shown in Figure 5(b) were extracted from the low resolution photon energy scan (Figure 2) covering the range from 20 eV to 40 eV, i.e., above the region of strong resonances. In this case, the contributions from the A and the B band are shown together since at high electron kinetic energy it becomes increasingly difficult to separate their respective contributions due to the decreased resolution of our spectrometer. The figure also shows data from (e,2e) measurements by Brion and Tan (circles),[27] and synchrotron measurements by Gustafsson *et al.*[32] (triangles) for comparison. One clearly sees some discrepancies between our data and the literature values. Our data exhibit a fairly constant contribution from the A + B bands, and a decreasing contribution of the X band towards higher photon energy. On the other hand, Refs. 27 and 32 show a decreasing contribution of the A + B bands, while the X band has a flatter photon energy dependence. The resolution in the work by Brion and Tan[27] was 1.3 eV

and a fitting procedure was needed to separate the different contributions. In the work by Gustaffson *et al.*,[32] the kinetic energy resolution was 0.3 eV, but the extracted branching ratio values depend linearly on the value of the asymmetry parameter which was not determined, therefore adding an additional uncertainty to their data. The kinetic energy resolution in our data changes approximately from 0.27 eV at 20 eV to 0.52 eV at 40 eV, respectively, being comparable to that of Ref. 32. Furthermore, since in a VMI measurement all electrons are accelerated to a uniform high impact energy, a bias in the detection probability of high/low kinetic energy electrons is not expected. The error bars for our measurement were estimated by varying slightly the energy intervals over which the integration of the different electronic bands was carried out and calculating differences between results from the four quadrants of our detector. Only contributions from the four valence bands were taken for the calculation, neglecting contributions to the total yield from multi-electron excitation.

Additionally, the results of 5(a) and 5(b) are quite consistent, making a comparison at 20 eV. The contribution of the A and B channels are the same in both measurements within experimental error. There is a mismatch however in the contribution of the X and C bands which could be due to a stronger background signal in the measurements of the low resolution scan, slightly affecting the results of the integration. However, the trend in the behaviour of the branching ratios is consistent in both scans and the reason for the disagreement with the previously published work remains unclear.

3. Branching ratios between vibrational levels and asymmetry parameters

Our high resolution scan allows determining the branching ratios and asymmetry parameters of the different vibrational levels within one electronic band. For the CO_2^+ ground state, the most complete analysis was so far published by Parr *et al.*,[33] whose results are also available online.[34] On the basis of our high resolution scan shown in Figure 3, the branching ratio of the vibrational ground state (000) of the X $^2\Pi_g$ band was retrieved following a similar fitting procedure as outlined in Refs. 33 and 34. Figure 6(a) shows a comparison between the branching ratios resulting from our work and the work by Parr *et al.*. The agreement between the two data sets is remarkably good. However, below 15 eV and above 18 eV, they clearly depart from each other. At high photon energies, the decrease in resolution causes an overlap in our VMI measurements between the contributions from different vibrational levels and reduces the reliability of our fitting procedure. The reason for the lower branching ratio observed below 15 eV with the VMI is somewhat unclear. Although the extraction voltages were not optimized for this particular kinetic energy range, the resolution of our instrument in that region is better than 65 meV, which is clearly sufficient to resolve the vibrational levels and comparable to that of Ref. 33.

In single photon ionization, the differential cross section in a plane containing the polarization axis is

$$\frac{d\sigma}{d\Omega} = \frac{\sigma}{4\pi}\left(1 + \frac{\beta}{2}(3\cos^2\theta - 1)\right),$$
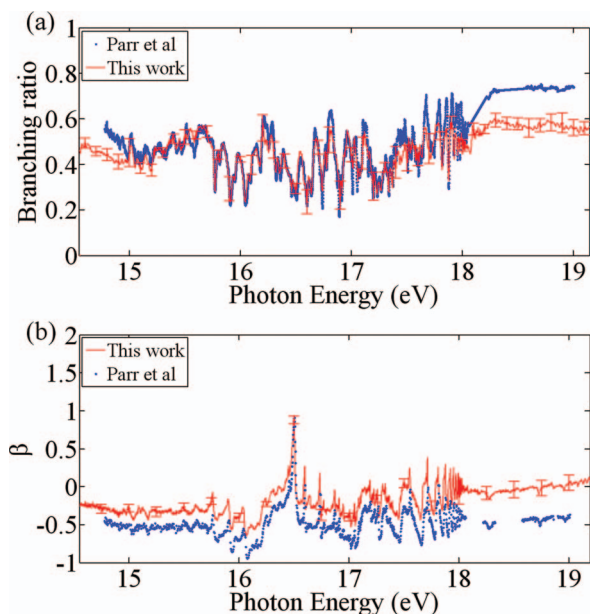
FIG. 6. Branching ratio (a) and asymmetry parameter (b) for the first vibrational level of the ionic ground state. The red curve corresponds to our data-set while the blue dots were taken from Ref. 34.

FIG. 7. Branching ratios and asymmetry parameters for selected vibrational levels of the A$^2\prod_u$ band. Steep variations are observed for photon energies below 18 eV, which are due to the excitation of intermediate resonant states.

where θ denotes the angle between the polarization axis of the light and the outgoing electron, and σ is the partial photoionization cross section for a particular vibrational channel. In Figure 6(b), the dependence of the asymmetry parameter β for the vibrational ground state (000) of the X band on the photon energy retrieved from our measurement is compared to the results from Refs. 33 and 34 The qualitative agreement between both measurements is remarkably good but there is an offset between the two curves that reaches a maximum beyond 18 eV. As a further test to validate our procedure, we measured the well-known anisotropy parameter for ionization of He atoms with 27.3 eV photons. The retrieved β value of 2.1 ± 0.1 shows that although in agreement with well-established values within experimental error, there is a small offset in the retrieved β value from our measurement. The disagreement may come from small distortions in our images originating from the electrostatic optics.

For the A, B, and C electronically excited valence states of CO$_2^+$ no detailed analysis of the vibrational branching ratios is available in the literature. Roy *et al.*[1] and Rathbone *et al.*[35] have studied the C$^2\Sigma_g^+$ state in the energy range from 20 eV to 28 eV and 20 eV to 110 eV, respectively. From the VMI data presented in Figure 3 the vibrational branching ratios and the vibrationally resolved β-parameters can be determined for the strongest channels of the A, B, and C bands, respectively.

Figure 7 shows the vibrational branching ratios (Figure 7(a)) and the asymmetry parameters β (Figure 7(b)) for the symmetric stretching mode (v$_1$00) of the A $^2\Pi_u$ state, which provide the strongest contribution to the electron yield, from the onset at 17.32 eV up to 21.2 eV. To separate the contributions from different vibrational states we have implemented a fitting procedure similar to the one employed to calculate the contribution of the ground vibrational level of the X state.[33,34] Beyond the onset of the B-band at 18.077 eV, it
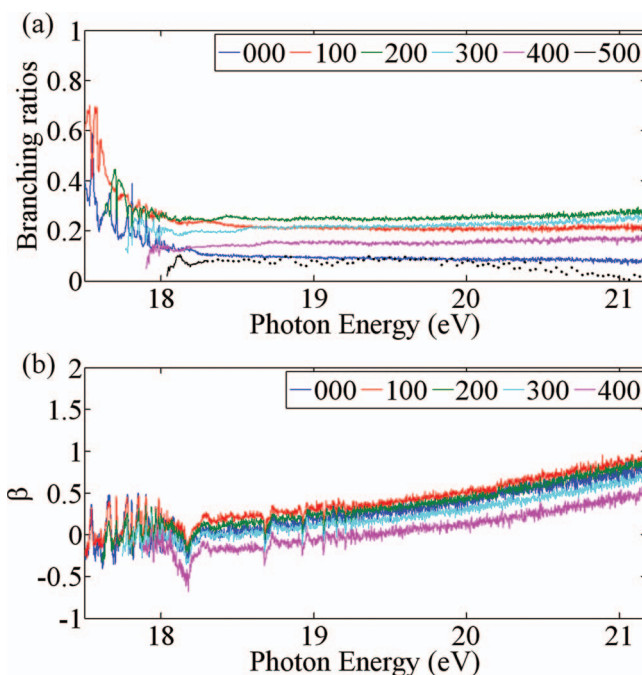
is difficult to separate the contribution of the (500) state from that of the very strong B-state ground vibrational level. For photon energies over 18.3 eV approximately, it is not possible to resolve the peak corresponding to the (500) state any longer and as a consequence the results of our fitting for this state are not so reliable in that photon energy region. In Figure 7, we have discriminated both regions by plotting with a solid and dotted line, respectively. Within our experimental accuracy, higher members of the (v$_1$00) progression and vibrational levels with other symmetries have a negligible contribution to the ionization yield. The branching ratios show a strong resonant structure up to the onset of the B-state and there is still some rearrangement in the contributions below the onset of the C-state. Towards higher photon energies, the branching ratios stay essentially constant and agree relatively well with Franck-Condon factors determined by Takeshita *et al.*[36] The asymmetry parameters have been determined for the first five members of the symmetric stretching mode of the A-state. For photon energies larger than approximately 18.5 eV, the asymmetry parameter for all the levels increase monotonically. Additionally, for a fixed photon energy, the different vibrational levels spread over an interval of asymmetry parameter values of <0.4. This behaviour is qualitatively in good agreement with calculations performed by Swanson *et al.*,[37] who attributed this monotonical increase with photon energy (up to 22.5 eV) and the vibrational state dependent spread to the presence of a π_g shape resonance at 20 eV. However, their calculations predict that at fixed photon energy, the asymmetry parameter decreases monotonically with increasing vibrational level while our observations show that the asymmetry parameter of the (000) level lies in between those of the (200) and the (300). Additionally, the values predicted by Swanson

et al. are on average 0.2 higher than our observations, which on the other hand, agree well within experimental accuracy to measurements performed by Grimm *et al.*[38] at selected photon energies, considering that our uncertainty interval in determining these values is on the order of 0.2.

When the ionization involves the excitation of super-excited or Rydberg states with a different symmetry of the electronic wave function vibronic interactions become strong. This can be seen in the region below the onset of the B-state and also around 19 eV where variations in the asymmetry parameters are visible, which are related to the resonances in the total electron yield shown in Figure 4(d). The strong dip in the asymmetry parameter around 18.08 eV, the onset of the B state, is an artefact. Around this region, the very high signal level produced a degradation of the images that affects the calculation of the asymmetry parameter, especially for those states close in energy to the onset of the B band.

The evolution of the branching ratios and asymmetry parameters with photon energy shown in Figure 7 is of high relevance for the validation of theoretical approaches seeking to model the photoionization process at these photon energies. These complex models in turn are highly relevant for the interpretation of the outcome of experiments in attosecond molecular science.

Figures 8 and 9 show the branching ratios and asymmetry parameters for selected vibrational levels of the B $^2\Sigma_u^+$ and C $^2\Sigma_g^+$ electronic bands, respectively. In these figures, we have included only the strongest vibrational levels, since these are the only ones we could identify unambiguously over the entire photon energy range covered. In both cases, the ground vibrational level is strongly dominant. The measured asymmetry parameter for (000) vibrational ground state of the C band shown in Figure 9 has a maximum value of 1.5 at 19.5 eV photon energy and decreases towards higher photon energies. This result is in good agreement with earlier
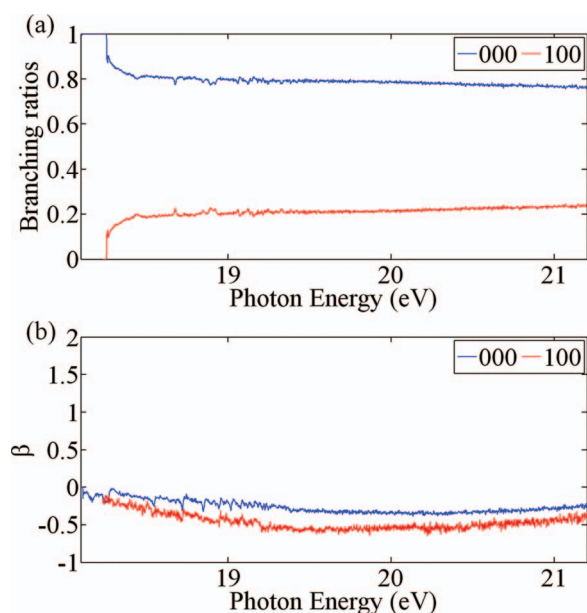

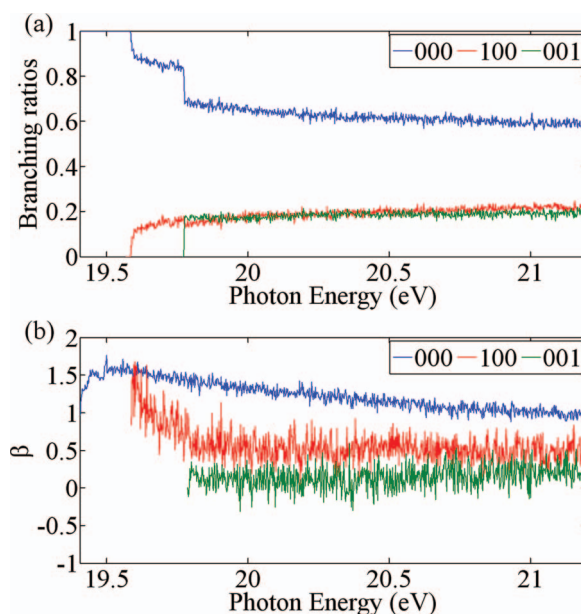FIG. 9. Branching ratios and asymmetry parameter for selected vibrational levels of the C$^2\Sigma_g^+$ band.

measurements.[1,35,38] The β parameter for the (100) state lies below the one of the (000) state which is unexpected since outside resonant regions the levels (000) and (100) should behave similarly. The asymmetry parameter of the (001) state shows a different behaviour. At threshold, it starts with a value around zero and increases towards higher photon energies. The asymmetry parameter of the (001) state has been studied first by Roy *et al.*,[1] who assigned it to the (101) combination band. Later, Rathbone *et al.*[35] reinvestigated the C-band and reassigned this particular vibrational state to the asymmetric stretching mode (001) supported by their own theoretical calculations and previous pulsed field ionization experiments. We follow their assignment and found that our values are qualitatively in good agreement with the experimental results obtained by Roy *et al.*[1] In principle, this state is dipole forbidden and it arises via mixing with the B $^2\Sigma_u^+$ state. Therefore, one expects a similar angular distribution as for the B-state, as indeed can be seen by comparing Figures 8 and 9.

The C-band provides the weakest contribution to the total yield, and since our measurements were not optimized for these particular states our data are rather noisy in that region. Moreover, by inspecting the branching ratios we observe that the contributions from the states (100) and (001) to the total yield are overestimated compared to Roy *et al.*,[1] due to the fact that the signal sits on a pedestal that becomes relevant for these rather weak signals. This might explain why our determination of the asymmetry parameter for the (100) level is lower than expected, since the measured contribution of the state to the total yield enters in our calculation to determine the asymmetry parameter. On the other hand, the asymmetry parameters for the vibrational ground states of the B and C-bands as already mentioned earlier are in good agreement with the results reported previously in the photon energy range where a comparison is possible.

FIG. 8. Branching ratios and asymmetry parameters for selected vibrational levels of the B$^2\Sigma_u^+$ band.

4. Slow photoelectrons spectrum

Photoelectron spectroscopy experiments typically employ a narrowband source with a photon energy high enough to induce ionization. The measured spectra then contain contributions from all accessible energy levels, which can be identified by analyzing the kinetic energy of the measured electrons. The resolution when using this approach is at best a few meV. In order to overcome this limitation, one can restrict the detection to electrons with zero (or a very small) kinetic energy (Threshold Photoelectron Spectroscopy or TPES). Electrons with zero kinetic energy can only be formed when the photon energy matches the energy of a particular ionic state, which therefore can be directly identified.[39,40] However, the presence of auto-ionizing states yielding low kinetic energy electrons lowers the resolution and obscures the interpretation of the data.[41,42] By applying a delayed pulsed field extraction and gating in the detection process, the discrimination against non-zero kinetic energy electrons and — therefore — the resolution can be improved significantly. This technique has been called Zero Kinetic Energy (ZEKE) photoelectron spectroscopy and has allowed studying molecular systems with rotational state resolution.[43,44] It has later been understood that the delayed pulsed extraction field mostly ionizes long-lived high-n Rydberg states,[45,46] which acquire a long lifetime due to a combination of l- and m-mixing interactions.[47–51]

Recently a novel alternative to ZEKE and TPES has been introduced.[52,53] The technique, called slow photoelectron spectroscopy (SPES), is based on channel resolved photoelectron spectroscopy with tunable sources and allows recovering, among other things, the contribution of states with weak Franck-Condon factors by integrating the contributions of slow electrons (typically less than a few tens of meV in kinetic energy) to a particular state. SPES can be studied from our VMI data for photon energies below the first dissociation limit at 19.071 eV.[54] Figure 10 shows the SPES spectrum retrieved from electrons with kinetic energy lower than 55 meV in the region between the onset of the A band and the onset of the B band. The spectrum shows a rich structure in which for instance, the spin-orbit splitting of the vibrational progression $(v_1 00)$ of the A band can be resolved. The results can be compared to the pulsed field ionization high resolution data from Liu *et al.*[5] and the TPES studies of Frey *et al.*,[55] and Baer and Guyon.[7] Although the resolution in the VMI

is lower than in the pulsed field ionization results of Ref. 5, it is better than that reported in Ref. 7 (where the spin-orbit splitting was not resolved) and is comparable to the one of Ref. 55. Our data permit to identify some of the peaks present in Ref. 5, and therefore the line assignment in Figure 10 follows the assignments presented there. When comparing our SPES results to the results of Ref. 5, it is to be considered that the VMI measurements are performed in a dc extraction field of 116 V/cm. This lowers the ionization potential by an amount of $\Delta E(\text{cm}^{-1}) = 66$ cm^{-1} or 8 meV, and makes all spectral features appear a few meV lower energy than in Ref. 5. When considering the use of the VMI technique, we furthermore note the fact that VMI measurements always contain a small artefact at zero kinetic energy due to Coulomb focussing of the ejected photoelectrons by the ionic core left behind.[56,57] These effects are significant for photoelectrons that are ejected with a kinetic energy <15–25 meV in our setup, and do not affect photoelectrons with higher kinetic energies. Therefore, we can be assured that all spectral features appearing in Figure 10 are due to low kinetic energy electrons and do not correspond to artefacts.

The results of Figure 10 show that our instrument can resolve the spin-orbit splitting of the symmetric stretching vibrations in the A band, which are separated approximately by 95 cm^{-1} (=11.8 meV). The other assignments in the figure correspond to mixed states, in which one quanta of the bending mode and one or more quanta of the symmetric stretching are excited. In one case, the transition comes from the neutral ground state of the molecule while in the progression of mixed states, the transition originates from a vibrationally excited state of the neutral with one quanta of the bending mode. The observation of hot bands is due to the fact that our molecular sample was at room temperature, since at 300 K the Boltzmann factor for the (010) mode is 4%.

C. Evolution of a strong forbidden transition

The rich structure of peaks observed in Figure 10 shows that in the vicinity of auto-ionizing resonances, the population of vibronic states is not given by Franck-Condon factors. In this section, we will elaborate on this, and will discuss a remarkable observation connected to the formation of the (410) vibrational level of the A-state.

As seen in Figure 3(b), the photoelectron spectrum of the A band is characterized by a marked predominance of vibrational levels corresponding to different quanta of excitation of the symmetric stretching mode $(v_1 00)$, since these transitions are characterized by strong Franck-Condon factors. However, in the vicinity of auto-ionizing resonances, additional vibrational levels become visible at low kinetic energies, as discussed in Sec. III B. In particular, it is possible to identify the $\kappa^2\Sigma^-(v_1 10)$ series ($v_1 = 1$–4). Our attention will be focused on the strongest peak of the series that is visible in Figure 10, the one at 17.942 eV, in the vicinity of the onset of the B band. This peak has been observed in several threshold photoelectron studies over the years.

In the very first studies by Batten *et al.*,[6] and Frey *et al.*,[55] the assignment remained unclear. Baer and Guyon,[7] studied
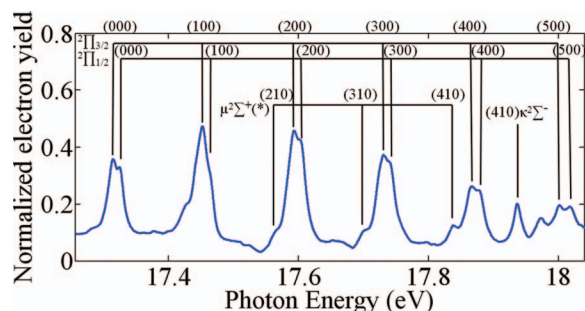

FIG. 10. Spectrum of slow photoelectrons (SPES) for the A-band. The assignments follow Ref. 5. (*) Transitions originating in the excited vibrational state $(010)^1\prod$ of the neutral.
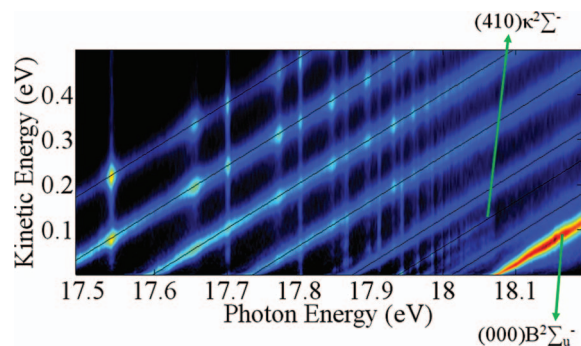
FIG. 11. Vibrational levels of the $A^2\Pi_u$ band (black solid lines) in the region around the ionization threshold of the $B^2\Sigma_u^+$ band. A sudden drop in the yield of the (410) $\kappa^2\Sigma^-$ is observed exactly at the onset of the B band.

the TPES of both the $^{12}CO_2$ and $^{13}CO_2$ isotopologs and found that this peak was only present in the $^{12}CO_2$ spectrum. They therefore concluded that this state may be a mixture of the $A^2\Pi_u$ and a^4B_1 level in a bent geometry, which can only be reached through a bent auto-ionizing state, since the Franck-Condon factors for direct ionization involving bending vibrations are extremely small. Following the line assignments of Ref. 5, this line corresponds to a transition from the ground state of the neutral molecule to the state (410) $\kappa^2\Sigma^-$, one of the four Renner-Teller and spin-orbit split components of the (410) vibrational mode. The intensity for this peak is remarkably high. Also in the spectrum measured by Liu *et al.*,[5] the (410) $\kappa^2\Sigma^-$ line has a relative intensity of almost 80% compared to the strongest line ((100) $^2\Pi_{3/2}$) in their spectrum of the A band. Figure 11 presents a contour plot showing the photoelectron spectra in the photon energy region below the onset of the B band, where the (410) $\kappa^2\Sigma^-$ appears. It is possible to observe that this state is not only present at very low kinetic energies, but instead, its contribution to the total yield is non-negligible up to the onset of the B band, where it seems to disappear suddenly.

To further inspect the behaviour of the (410) $\kappa^2\Sigma^-$ state and compare it to the $(v_1 00)$ progression, partial electron yields were calculated by integrating along the black lines indicated in Figure 11 with $\Delta E_{kin} = 1$ meV. The result is shown in Figure 12 together with the total electron yield in the interesting photon energy range between 17.88 eV to 18.15 eV. When comparing the partial electron yield (Figure 12(b)) originating from the symmetric stretching mode $(v_1 00)$, $v_1 = 0-2$, with the one from the (410) mode one notices that the resonant peaks that give rise to an enhancement of the $(v_1 00)$, $v_1 = 0-2$ formation (blue vertical lines in Figure 12(a)) are distinct from the resonant peaks that lead to formation of the (410) state (red vertical lines in Figure 12(a)). As inspection of Figure 4(c) shows, the enhancement in the partial electron yields belong to the Henning diffuse and sharp series. In particular, the peaks in the yield of the (410) state belong to the Henning sharp series, which only show up weakly in the yields of the $(v_1 00)$ progression.

As already stated in Sec. III B 1, the Henning series have been assigned to a Rydberg series converging to the $B\ ^2\Sigma_u^+$ band (green vertical line in Figure 12). In particular, the diffuse series corresponds to $ns\sigma_g\ ^1\Sigma_u^+$ where a $3\sigma_u$ electron is
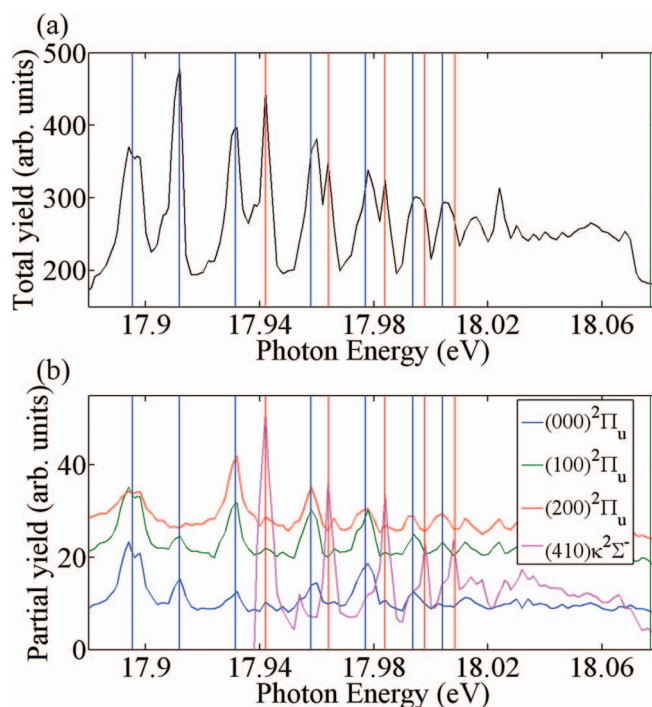

FIG. 12. Total yield (a) and partial yields of several vibrational states (b) belonging to the A band in the region 17.88–18.08 eV. The vertical lines indicate peaks positions; blue: peaks of the $(v_1 00)$ states; and red: peaks of the (410) state. The green solid vertical line marks the onset of the B band.

excited to an $ns\sigma_g$ orbital, while in the sharp series the $3\sigma_u$ electron is promoted to $nd\sigma_g\ ^1\Sigma_u^+$ Rydberg states. The onset of the (410) state at 17.942 eV coincides with the $n = 10$ level of the Henning sharp series. Therefore, it can be safely assumed, that the peaks in the partial electron yield of the (410) state at higher photon energies are induced by the Henning series with $n > 10$.

In theoretical calculations, Praet *et al.*[58] found that the geometry of the B-state is slightly bent with an angle of about $170°$. This bent structure probably also prevails for Rydberg series converging to the B-band. Thus, the excitation of the bending mode is facilitated by the intermediate $nd\sigma_g\ ^1\Sigma_u^+$ Rydberg states. This explains also the sharp drop of the partial electron yield at the onset of the B band. Why mainly the Henning sharp series contributes to the excitation of the (410) state remains an open question. Our interpretation of the formation of the (410) state is further supported by measurements of the anisotropy parameter, which are very similar for all $(v_1 00)$ states, but distinct for the contribution corresponding to the (410) state. This is shown in Figure 13, where the evolution of the asymmetry parameter shows that the (410) state oscillates out of phase with the respect to the asymmetry parameters of $(v_1 00)$ progression. In conclusion, the results shown in this section indicate that the presence of strong auto-ionizing resonances, such as the Henning series, significantly affects the distribution of vibrational populations of the ion. A similar analysis has been done before by Parr *et al.*,[59] and West *et al.*,[10] concentrating on the ionic ground state. In particular, Parr *et al.* followed the behaviour of branching ratios and asymmetry parameters of vibrational states of the X band around three resonances. Interestingly they also found that an
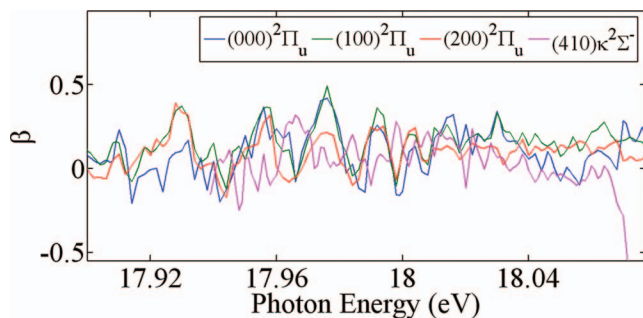
FIG. 13. Asymmetry parameter of several vibrational states belonging to the A band below the onset of the B band. The (410) state shows a different resonant behaviour compared to the ($v_1$00) series.

excitation of ($v_1$10) levels in the region of a Henning sharp resonance changes the distribution of vibrational populations. The works by Parr *et al.*, West *et al.*, others, and our own contributions here call for an attempt to model the observed experimental results.

IV. CONCLUSIONS

In this work, we have presented an overview of valence band photoionization of CO_2 as measured using synchrotron radiation and a VMI spectrometer. The combination of a continuous source of tunable photon energy in the VUV and XUV region of the electromagnetic spectrum and a VMI with an integrated gas injection system made it possible to acquire a vast amount of data in a relatively short time, recording simultaneously kinetic energy and angular distributions.

From the collected data it has been possible to retrieve the total photoelectron yield as a function of photon energy and to observe a large number of auto-ionizing resonances. The collected data have also allowed retrieving electronic and vibrational branching ratios, as well as the vibrationally resolved photoelectron angular distributions as a function of photon energy. Additionally the analysis of the low energy electrons in our data shows a rich structure close to resonant regions, as well as the presence of hot bands and forbidden transitions. In particular, we have shown for the first time the evolution of the state (410) $\kappa^2\sum^-$ belonging to the A electronic band, which was a source of rich debate in the literature. Our data clearly confirm the explanation that the strength of the state at threshold is due to the presence of a resonance, and that in off-resonance regions the weak Franck-Condon factors make the contribution of this state almost negligible.

In the context of the growing field of attosecond molecular science, the results shown here demonstrate that the analysis and interpretation of experimental results from pump-probe experiments should not fail to include the effects of auto-ionizing states when the photon energy of the ionizing source falls in the resonant region. Any analysis of this kind will necessarily call for a renewed effort to model the photoionization process in molecular systems, including the interaction between nuclear and electronic degrees of freedom and resonant intermediate processes. The experimental results presented here and in the references may serve as a tool to validate those theoretical models.

[1]P. Roy, R. J. Bartlett, W. J. Trela, T. A. Ferrett, A. C. Parr, S. H. Southworth, J. E. Hardis, V. Schmidt, and J. L. Dehmer, J. Chem. Phys. **94**, 949 (1991).

[2]A. C. Parr, P. M. Dehmer, J. L. Dehmer, K. Ueda, J. B. West, M. R. F. Siggel, and M. A. Hayes, J. Chem. Phys. **100**, 8768 (1994).

[3]T. Masuoka, Phys. Rev. A **50**, 3886 (1994).

[4]P. Baltzer, F. T. Chau, J. H. D. Eland, L. Karlsson, M. Lundqvist, J. Rostas, K. Y. Tam, H. Veenhuizen, and B. Wannberg, J. Chem. Phys. **104**, 8922 (1996).

[5]J. B. Liu, M. Hochlaf, and C. Y. Ng, J. Chem. Phys. **113**, 7988 (2000).

[6]C. F. Batten, J. A. Taylor, and G. G. Meisels, J. Chem. Phys. **65**, 3316 (1976).

[7]T. Baer and P. M. Guyon, J. Chem. Phys. **85**, 4765 (1986).

[8]D. A. Shaw, D. M. P. Holland, M. A. Hayes, M. A. Macdonald, A. Hopkirk, and S. M. McSweeney, Chem. Phys. **198**, 381 (1995).

[9]D. M. P. Holland, J. B. West, and M. A. Hayes, Chem. Phys. **148**, 241 (1990).

[10]J. B. West, M. A. Hayes, M. R. F. Siggel, J. L. Dehmer, P. M. Dehmer, A. C. Parr, and J. E. Hardis, J. Chem. Phys. **104**, 3923 (1996).

[11]F. Krausz and M. Ivanov, Rev. Mod. Phys. **81**, 163 (2009).

[12]G. Sansone, F. Kelkensberg, J. F. Perez-Torres, F. Morales, M. F. Kling, W. Siu, O. Ghafur, P. Johnsson, M. Swoboda, E. Benedetti, F. Ferrari, F. Lepine, J. L. Sanz-Vicario, S. Zherebtsov, I. Znakovskaya, A. L'Huillier, M. Y. Ivanov, M. Nisoli, F. Martin, and M. J. J. Vrakking, Nature (London) **465**, 763 (2010).

[13]W. Siu, F. Kelkensberg, G. Gademann, A. Rouzée, P. Johnsson, D. Dowek, M. Lucchini, F. Calegari, U. De Giovannini, A. Rubio, R. R. Lucchese, H. Kono, F. Lépine, and M. J. J. Vrakking, Phys. Rev. A **84**, 063412 (2011).

[14]O. Smirnova, Y. Mairesse, S. Patchkovskii, N. Dudovich, D. Villeneuve, P. Corkum, and M. Y. Ivanov, Nature (London) **460**, 972 (2009).

[15]D. Shafir, H. Soifer, B. D. Bruner, M. Dagan, Y. Mairesse, S. Patchkovskii, M. Y. Ivanov, O. Smirnova, and N. Dudovich, Nature (London) **485**, 343 (2012).

[16]A. T. J. B. Eppink and D. H. Parker, Rev. Sci. Instrum. **68**, 3477 (1997).

[17]D. M. P. Holland and D. A. Shaw, J. Electron Spectrosc. Relat. Phenom. **184**, 144 (2011).

[18]P. O'Keeffe, P. Bolognesi, A. Moise, R. Richter, Y. Ovcharenko, and L. Avaldi, J. Chem. Phys. **136**, 104307 (2012).

[19]O. Ghafur, W. Siu, P. Johnsson, M. F. Kling, M. Drescher, and M. J. J. Vrakking, Rev. Sci. Instrum. **80**, 033110 (2009).

[20]P. Baumgärtel, see http://www.helmholtz-berlin.de.

[21]G. Reichardt, J. Bahrdt, J. S. Schmidt, W. Gudat, A. Ehresmann, R. Müller-Albrecht, H. Molter, H. Schmoranzer, M. Martins, N. Schwentner, and S. Sasaki, Nucl. Instrum. Methods Phys. Res. A **467**, 462 (2001).

[22]J. W. Gallagher, C. E. Brion, J. A. R. Samson, and P. W. Langhoff, J. Phys. Chem. Ref. Data **17**, 9 (1988).

[23]M. J. J. Vrakking, Rev. Sci. Instrum. **72**, 4084 (2001).

[24]V. Dribinski, A. Ossadtchi, V. A. Mandelshtam, and H. Reisler, Rev. Sci. Instrum. **73**, 2634 (2002).

[25]G. A. Garcia, L. Nahon, and I. Powis, Rev. Sci. Instrum. **75**, 4989 (2004).

[26]L. S. Wang, J. E. Reutt, Y. T. Lee, and D. A. Shirley, J. Electron Spectrosc. Relat. Phenom. **47**, 167 (1988).

[27]C. E. Brion and K. H. Tan, Chem. Phys. **34**, 141 (1978).

[28]H. J. Freund, H. Kossmann, and V. Schmidt, Chem. Phys. Lett. **123**, 463 (1986).

[29]B. Kovac, J. Chem. Phys. **78**, 1684 (1983).

[30]J. H. D. Eland and J. Berkowitz, J. Chem. Phys. **67**, 2782 (1977).

[31]C. Fridh, L. Asbrink, and E. Lindholm, Chem. Phys. **27**, 169 (1978).

[32]T. Gustafsson, E. W. Plummer, D. E. Eastman, and W. Gudat, Phys. Rev. A **17**, 175 (1978).

[33]A. C. Parr, J. B. West, M. R. F. King, K. Ueda, P. M. Dehmer, and J. L. Dehmer, J. Res. Natl. Inst. Stand. Technol. **106**, 795 (2001).

[34] A. C. Parr, J. B. West, M. R. F. King, K. Ueda, P. M. Dehmer, J. L. Dehmer, D. J. Schwab, A. M. Sansonetti, K. Olsen, and R. A. Dragoset, see http://www.nist.gov/pml/data/co2/index.cfm.

[35] G. J. Rathbone, E. D. Poliakoff, J. D. Bozek, R. R. Lucchese, and P. Lin, J. Chem. Phys. **120**, 612 (2004).

[36] K. Takeshita, N. Shida, and E. Miyoshi, J. Chem. Phys. **112**, 10838 (2000).

[37] J. R. Swanson, D. Dill, and J. L. Dehmer, J. Phys. B **14**, L207 (1981).

[38] F. A. Grimm, J. John D. Allen, T. A. Carlson, M. O. Krause, D. Mehaffy, P. R. Keller, and J. W. Taylor, J. Chem. Phys. **75**, 92 (1981).

[39] E. W. Schlag, W. B. Peatman, and K. Müller-Dethlefs, J. Electron Spectrosc. Relat. Phenom. **66**, 139 (1993).

[40] K. Müller-Dethlefs and E. W. Schlag, Annu. Rev. Phys. Chem. **42**, 109 (1991).

[41] P. M. Guyon, T. Baer, and I. Nenner, J. Chem. Phys. **78**, 3665 (1983).

[42] T. Baer, Adv. Chem. Phys. **64**, 111 (1986).

[43] K. Müller-Dethlefs, M. Sander, and E. W. Schlag, Z. Naturforsch. **39a**, 1089 (1984).

[44] K. Müller-Dethlefs, M. Sander, and E. W. Schlag, Chem. Phys. Lett. **112**, 291 (1984).

[45] C. Bordas, P. F. Brevet, M. Broyer, J. Chevaleyre, P. Labastie, and J. P. Perrot, Phys. Rev. Lett. **60**, 917 (1988).

[46] C. R. Mahon, G. R. Janik, and T. F. Gallagher, Phys. Rev. A **41**, 3746 (1990).

[47] W. A. Chupka, J. Chem. Phys. **98**, 4520 (1993).

[48] M. J. J. Vrakking, I. Fischer, D. M. Villeneuve, and A. Stolow, J. Chem. Phys. **103**, 4538 (1995).

[49] M. J. J. Vrakking and Y. T. Lee, J. Chem. Phys. **102**, 8818 (1995).

[50] M. J. J. Vrakking and Y. T. Lee, J. Chem. Phys. **102**, 8833 (1995).

[51] M. J. J. Vrakking and Y. T. Lee, Phys. Rev. A **51**, R894 (1995).

[52] M. Briant, L. Poisson, M. Hochlaf, P. de Pujo, M.-A. Gaveau, and B. Soep, Phys. Rev. Lett. **109**, 193401 (2012).

[53] J. C. Poully, J. P. Schermann, N. Nieuwjaer, F. Lecomte, G. Gregoire, C. Desfrancois, G. A. Garcia, L. Nahon, D. Nandi, L. Poisson, and M. Hochlaf, Phys. Chem. Chem. Phys. **12**, 3566 (2010).

[54] R. Bombach, J. Dannacher, J. P. Stadelmann, and J. C. Lorquet, J. Chem. Phys. **79**, 4214 (1983).

[55] R. Frey, B. Gotchev, O. F. Kalman, W. B. Peatman, H. Pollak, and E. W. Schlag, Chem. Phys. **21**, 89 (1977).

[56] C. Bordas, Phys. Rev. A **58**, 400 (1998).

[57] C. Nicole, I. Sluimer, F. Rosca-Pruna, M. Warntjes, M. Vrakking, C. Bordas, F. Texier, and F. Robicheaux, Phys. Rev. Lett. **85**, 4024 (2000).

[58] M. T. Praet, J. C. Lorquet, and G. Raseev, J. Chem. Phys. **77**, 4611 (1982).

[59] A. C. Parr, D. L. Ederer, J. L. Dehmer, and D. M. P. Holland, J. Chem. Phys. **77**, 111 (1982).